

# Raman transitions without adiabatic elimination: A simple and accurate treatment

Rui HAN<sup>a</sup>, Hui Khoon NG<sup>a,b</sup> and Berthold-Georg ENGLERT<sup>a,c</sup>

<sup>a</sup>*Centre for Quantum Technologies, National University of Singapore, Singapore 117543, Singapore*

<sup>b</sup>*DSO National Laboratories, 20 Science Park Drive, Singapore 118230, Singapore*

<sup>c</sup>*Department of Physics, National University of Singapore, Singapore 117542, Singapore*

(Posted on the arXiv on 28 September 2012)

Driven Raman processes — nearly resonant two-photon transitions through an intermediate state that is non-resonantly coupled and does not acquire a sizeable population — are commonly treated with a simplified description in which the intermediate state is removed by adiabatic elimination. While the adiabatic-elimination approximation is reliable when the detuning of the intermediate state is quite large, it cannot be trusted in other situations, and it does not allow one to estimate the population in the eliminated state. We introduce an alternative method that keeps all states in the description, without increasing the complexity by much. An integro-differential equation of Lippmann-Schwinger type generates a hierarchy of approximations, but very accurate results are already obtained in the lowest order.

**Keywords:** Raman transition; adiabatic elimination; Rydberg excitation

## 1. Introduction

Atomic and molecular systems can be coupled in various ways, so that the atomic states evolve and the populations of states change. Of all the electromagnetic multipole couplings, the electric dipole is the strongest. Thus optically allowed atomic transitions are often stimulated by an electric-dipole coupling between the atom and a well-controlled laser.

Dipole-allowed transitions can be driven with optical lasers directly. It is, however, quite common that the desired transition is dipole forbidden or the transition frequency is outside of the popular optical range. Then some intermediate state can assist in an indirect transition. Examples for such processes include three-level Raman transitions (1), multi-level Raman transitions (2, 3), and stimulated Raman adiabatic passage (STIRAP) (4, 5). They all have their useful applications, with three-level Raman transitions being perhaps the most widely used in a large variety of experiments.

In order to reduce the computational complexity of dealing with large Hilbert spaces, one can decrease the dimensionality of the system by eliminating states that are not populated much or not coupled strongly. For a typical three-level Raman transition, the intermediate state is far off-resonantly coupled to the relevant initial and target states. This enables one to perform the so-called *adiabatic elimination* that gets rid of the less relevant state and yields a two-level effective Hamiltonian. Although the procedure of adiabatic elimination is well understood — see (6) and (7), for instance — it gives a reliable approximation only when the detuning of the intermediate state is much larger than the Rabi frequencies for the coupling to the other two states.

In this paper, we introduce an alternative approach to the quantitative description of the three-level Raman transition. This new method does not rely on adiabatic elimination and gives a much more accurate solution while the computational complexity remains low. We set the stage in Section 2, where we briefly review driven three-level systems and state the notational conventions used throughout. Then, Section 3 deals with the usual adiabatic-elimination approach and

comments on its limitations and problems. Our new approach is explained in Section 4: First we present the general methodology, then we show how it gives the exact solution to the resonant two-photon transition problem, and finally we generate reliable approximations for the situation of a non-resonant two-photon transition. We close with a summary and outlook.

## 2. The three-level system

A Raman transition is a two-photon process that gives an effective coupling between two states  $|0\rangle$  and  $|1\rangle$  via a far-detuned auxiliary state  $|e\rangle$ ; see Fig. 1. As mentioned above, Raman transitions are often used when the transition between levels  $|0\rangle$  and  $|1\rangle$  is dipole forbidden or has an inconvenient frequency. The  $\Lambda$ -type configuration of Fig. 1(a) applies to transitions between different ground states via an excited state; the cascade-type configuration of Fig. 1(b) can be used to achieve the transition between a ground state and a highly excited state, such as a Rydberg state. There is also a V-type transition with the level configuration similar to that of an inverted  $\Lambda$ -type transition. Although the level structures are different for these configurations, the underlying physics is essentially the same.

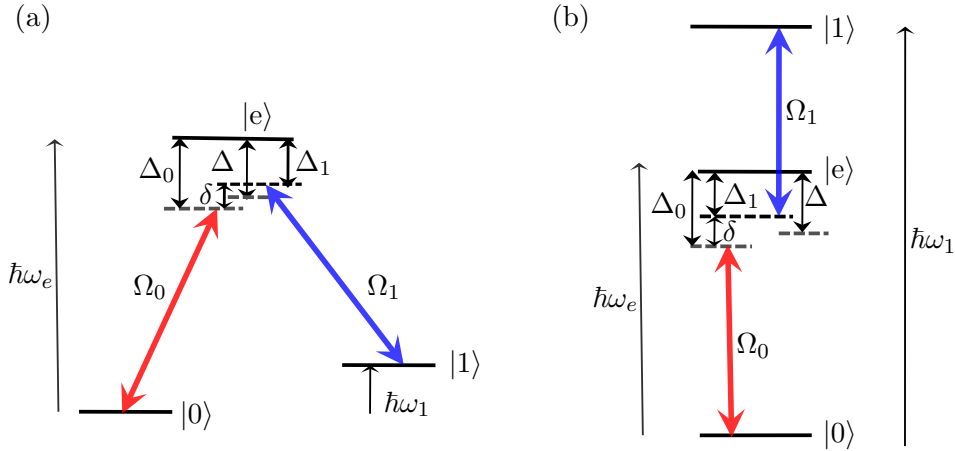


Figure 1. Level scheme of a typical Raman transition. (a) shows the level structure of a  $\Lambda$ -type Raman transition and (b) shows the level structure of a cascade-type Raman transition.  $\Omega_0$  and  $\Omega_1$  denote the Rabi frequencies of the individual two-level transitions,  $\Delta$  denotes the detuning of the laser from the transition frequency of the excited state and  $\delta$  is the detuning of the two-photon transition. The requirement is that the detuning  $\Delta$  is much larger than the Rabi frequencies so that the excited state  $|e\rangle$  is not significantly populated.

We will, therefore, restrict ourselves to treating the  $\Lambda$ -type Raman transition in detail. With reference to  $|0\rangle$ ,  $|1\rangle$ , and  $|e\rangle$  in this order, the  $3 \times 3$  matrix for the Hamiltonian of the system is

$$H = H_{\text{Atom}} + H_{\text{AL}}, \quad (1)$$

where

$$H_{\text{Atom}} = \hbar \begin{pmatrix} 0 & 0 & 0 \\ 0 & \omega_1 & 0 \\ 0 & 0 & \omega_e \end{pmatrix} \quad (2)$$

is the part for the atom by itself with the convention that the state  $|0\rangle$  has energy zero, and

$$H_{\text{AL}} = \frac{\hbar}{2} \begin{pmatrix} 0 & 0 & \Omega_0 e^{i\omega_{L0}t} \\ 0 & 0 & \Omega_1 e^{i\omega_{L1}t} \\ \Omega_0^* e^{-i\omega_{L0}t} & \Omega_1^* e^{-i\omega_{L1}t} & 0 \end{pmatrix} \quad (3)$$

accounts for the atom-laser interaction. The laser frequencies are denoted by  $\omega_{L0}$  and  $\omega_{L1}$ , respectively. The Rabi frequencies for the electric-dipole transitions are

$$\Omega_0 = \frac{q_{\text{el}}}{\hbar} \langle 0 | \mathbf{r} \cdot \mathbf{E}_{L0} | e \rangle \quad \text{and} \quad \Omega_1 = \frac{q_{\text{el}}}{\hbar} \langle 1 | \mathbf{r} \cdot \mathbf{E}_{L1} | e \rangle, \quad (4)$$

where  $q_{\text{el}}$  is the electron charge,  $\mathbf{E}_{L0}$  and  $\mathbf{E}_{L1}$  are the amplitudes of the electric fields of the laser beams and  $\mathbf{r}$  is the position vector of the atom. Each Rabi frequency depends on the intensity and polarization of the corresponding laser as well as the dipole matrix element between the two coupled states, and can be complex. Typically, the detuning  $\Delta$  is designed to be large, i.e.,  $|\Delta| \gg |\Omega_0|, |\Omega_1|$ , so that the auxiliary state  $|e\rangle$  does not get populated to avoid problems arising from uncontrolled spontaneous emission from  $|e\rangle$  to other states; see Fig. 1. Since the two-photon transition from  $|0\rangle$  to  $|1\rangle$  is nearly resonant, the overall detuning  $\delta$  of the two-photon transition is small compared with the average detuning  $\Delta$ ,  $|\delta/\Delta| \ll 1$ . If the detunings between the lasers and the atomic frequencies are denoted by  $\Delta_0 = \omega_e - \omega_{L0}$  and  $\Delta_1 = \omega_e - \omega_1 - \omega_{L1}$ , we have  $\Delta = (\Delta_0 + \Delta_1)/2$  and  $\delta = \Delta_0 - \Delta_1$ .

In view of the time-dependent phase factors in  $H_{\text{AL}}$ , it is expedient to switch to an interaction picture in which the Hamiltonian does not depend on time. This is achieved by identifying the “free” Hamiltonian  $H_0$  by a suitable splitting of the atomic Hamiltonian,

$$H_0 = H_{\text{Atom}} + \hbar \begin{pmatrix} \frac{1}{2}\delta & 0 & 0 \\ 0 & -\frac{1}{2}\delta & 0 \\ 0 & 0 & -\Delta \end{pmatrix} = \hbar \begin{pmatrix} \frac{1}{2}\delta & 0 & 0 \\ 0 & \omega_1 - \frac{1}{2}\delta & 0 \\ 0 & 0 & \omega_e - \Delta \end{pmatrix}, \quad (5)$$

for which we obtain the interaction-picture Hamiltonian

$$H_I = e^{iH_0 t/\hbar} (H - H_0) e^{-iH_0 t/\hbar} = \frac{\hbar}{2} \begin{pmatrix} -\delta & 0 & \Omega_0 \\ 0 & \delta & \Omega_1 \\ \Omega_0^* & \Omega_1^* & 2\Delta \end{pmatrix}. \quad (6)$$

The evolution of the three-level system is then studied with the aid of the Schrödinger equation

$$i\hbar \frac{\partial}{\partial t} \Psi_I(t) = H_I \Psi_I(t) \quad \text{with} \quad \Psi_I(t) = \begin{pmatrix} c_0(t) \\ c_1(t) \\ c_e(t) \end{pmatrix} = e^{iH_0 t/\hbar} \Psi(t), \quad (7)$$

where the components of  $\Psi_I(t)$  are the interaction-picture probability amplitudes for  $|0\rangle$ ,  $|1\rangle$ , and  $|e\rangle$ , related to the respective components of  $\Psi(t)$ , the amplitudes in the Schrödinger picture, by simple time-dependent phase factors. As a consequence of this simple relation between the components of  $\Psi(t)$  and  $\Psi_I(t)$ , we can simply square  $c_0(t)$ ,  $c_1(t)$ , or  $c_e(t)$  to obtain the probability amplitudes for the respective atomic levels, as exemplified by the probability for  $|0\rangle$ ,

$$\left| (1 \ 0 \ 0) \Psi(t) \right|^2 = \left| (1 \ 0 \ 0) \Psi_I(t) \right|^2 = |c_0(t)|^2, \quad (8)$$

where, of course,  $(1 \ 0 \ 0)$  is the three-component row for  $\langle 0|$ .

To understand the system analytically, we can solve for the eigensystem of this time-independent Hamiltonian directly. However, very often, this is neither the most efficient way

of getting the solution, nor the best method for obtaining a good physical insight into the system. Various approaches have been developed, of which the adiabatic elimination and, for  $\delta = 0$ , the dark-state method (8) are particularly useful and popular.

### 3. Adiabatic elimination

#### 3.1. The methodology

The standard textbook approach to the Raman-transition problem makes use of “adiabatic elimination” in accordance with the following line of reasoning. Since the excited state  $|e\rangle$  is far-detuned by  $\Delta$ , it will remain barely populated if it has no initial population. Thus, the change of the population in this state can be taken as approximately zero,  $\frac{\partial}{\partial t}c_e(t) = 0$ , so that

$$2i\frac{\partial}{\partial t}c_e(t) = \Omega_0^*c_0(t) + \Omega_1^*c_1(t) + 2\Delta c_e(t) = 0, \quad (9)$$

in view of the Schrödinger equation (7). We can now express  $c_e(t)$  as a linear combination of  $c_0(t)$  and  $c_1(t)$ , and so eliminate  $c_e(t)$  from the equations of motion for  $c_0(t)$  and  $c_1(t)$ . This gives us an effective  $2 \times 2$  Hamiltonian for the evolution of the two relevant states

$$H_{\text{eff}} = -\frac{\hbar}{2} \begin{pmatrix} \delta + \frac{|\Omega_0|^2}{2\Delta} & \frac{\Omega_0\Omega_1^*}{2\Delta} \\ \frac{\Omega_1\Omega_0^*}{2\Delta} & -\delta + \frac{|\Omega_1|^2}{2\Delta} \end{pmatrix} \quad \text{for} \quad i\hbar\frac{\partial}{\partial t}\psi(t) = H_{\text{eff}}\psi(t) \quad \text{with} \quad \psi(t) = \begin{pmatrix} c_0(t) \\ c_1(t) \end{pmatrix}. \quad (10)$$

As an immediate benefit of applying adiabatic elimination on the intermediate auxiliary state, the effective Hamiltonian is a simple  $2 \times 2$  matrix, for which the eigenvalues and the projectors to the eigenspaces are readily available.

The eigenvalues of  $H_{\text{eff}}$  are

$$E_{\pm} = -\frac{\hbar}{8\Delta}(|\Omega_0|^2 + |\Omega_1|^2) \pm \frac{\hbar}{2}\Omega_R \quad (11)$$

with the positive frequency  $\Omega_R$  given by

$$\Omega_R^2 = \frac{1}{(4\Delta)^2}(|\Omega_0|^2 + |\Omega_1|^2)^2 + \frac{\delta}{2\Delta}(|\Omega_0|^2 - |\Omega_1|^2) + \delta^2. \quad (12)$$

The projectors to the corresponding eigenspaces are  $\frac{1}{2}(1 \pm \sigma_o)$ , where

$$\sigma_o = \frac{2H_{\text{eff}} - E_+ - E_-}{E_+ - E_-} \quad (13)$$

is a Pauli-type matrix. If the evolution starts with all the population in the ground state  $|0\rangle$ , i.e.,  $c_0(t=0) = 1$ , the population in state  $|1\rangle$  at a later time  $t$  is

$$|c_1(t)|^2 = \frac{|\Omega_0|^2|\Omega_1|^2}{8\Delta^2\Omega_R^2} [1 - \cos(\Omega_R t)]. \quad (14)$$

This tells us the physical significance of  $\Omega_R = (E_+ - E_-)/\hbar$ : It is the effective Rabi frequency of the transition between states  $|0\rangle$  and  $|1\rangle$  via this Raman process.

In the situation of vanishing overall detuning,  $\delta = 0$ , we have

$$|c_1(t)|^2 = \frac{2|\Omega_0|^2|\Omega_1|^2}{(|\Omega_0|^2 + |\Omega_1|^2)^2} \left[ 1 - \cos \left( \frac{|\Omega_0|^2 + |\Omega_1|^2}{4\Delta} t \right) \right], \quad (15)$$

where the effective Rabi frequency is  $\Omega_R = (|\Omega_0|^2 + |\Omega_1|^2)/(4|\Delta|)$  and the amplitude of the Rabi oscillation is less than unity,

$$\frac{4|\Omega_0|^2|\Omega_1|^2}{(|\Omega_0|^2 + |\Omega_1|^2)^2} < 1, \quad (16)$$

unless  $|\Omega_0|^2 = |\Omega_1|^2$ . In other words, when  $\delta = 0$ , we get complete population transfer between state  $|0\rangle$  and state  $|1\rangle$  only if the two lasers drive the respective transitions equally strongly.

More generally, perfect population transfer from  $|0\rangle$  to  $|1\rangle$  is only possible if the two diagonal matrix elements of the effective Hamiltonian are identical, i.e., if there is no effective detuning after the adiabatic elimination. Then  $|0\rangle$  and  $|1\rangle$  are equal-weight superpositions of the eigenstates of  $H_{\text{eff}}$  and temporal evolution turns one into the other. For given laser intensities, and thus given Rabi frequencies  $\Omega_0$  and  $\Omega_1$ , the experimenter can exploit the Zeeman or the Stark effect to adjust the overall detuning such that

$$\delta = \frac{|\Omega_1|^2 - |\Omega_0|^2}{4\Delta}. \quad (17)$$

This makes the effective detuning vanish and ensures perfect population transfer. Indeed, for this value of  $\delta$ , the right-hand side of (14) simplifies,

$$|c_1(t)|^2 = \frac{1}{2} [1 - \cos(\Omega_R t)] \quad \text{with} \quad \Omega_R = \frac{|\Omega_0||\Omega_1|}{2|\Delta|}. \quad (18)$$

In experiments, specifically for two-photon population transfer from the ground state to a Rydberg state where the Rabi frequencies  $|\Omega_0|$  and  $|\Omega_1|$  can be an order of magnitude different in strengths, adjusting the detuning in accordance with (17) is important (9).

### 3.2. Light shift

When an atomic transition is driven by an electromagnetic radiation field with detuning  $\Delta$ , the dressed atomic levels are shifted. This is the so-called *light shift* of the atomic levels, which is a second-order correction to the eigenenergies of the Hamiltonian (10). If an atomic transition is driven by Rabi frequency  $\Omega$  with detuning  $\Delta$ , the light shift of the ground state of the transition is  $-|\Omega|^2/(4\Delta)$  and the light shift of the dressed excited state is of the same amount but opposite in sign. The overall light shift is a direct summation of the light shifts arising from individual electromagnetic radiation fields, when the atomic level is addressed by multiple fields.

In the present context, the light shift of state  $|0\rangle$  is  $\hbar\delta_0 = -\hbar|\Omega_0|^2/(4\Delta_0)$  and the light shift of state  $|1\rangle$  is  $\hbar\delta_1 = -\hbar|\Omega_1|^2/(4\Delta_1)$ . Thus, the value of  $\delta$  that brings the two-photon transitions into resonance is determined by

$$\delta = \frac{|\Omega_1|^2}{4\Delta + 2\delta} - \frac{|\Omega_0|^2}{4\Delta - 2\delta}, \quad (19)$$

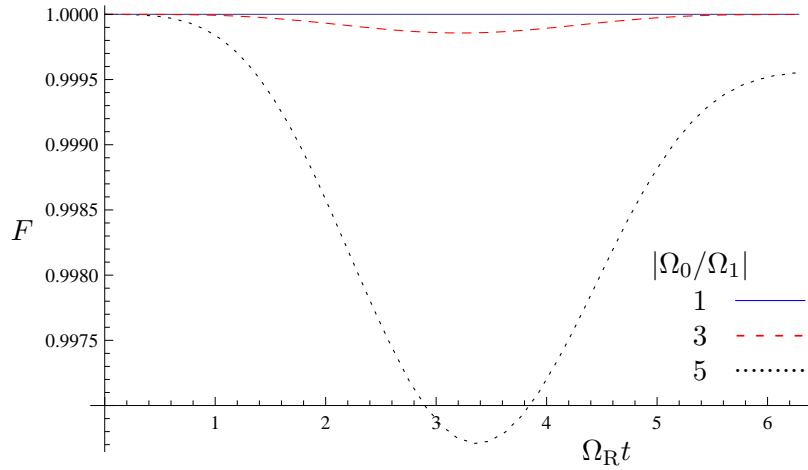


Figure 2. Fidelity between the two states at later time evolving with the exact Hamiltonian but for the two different  $\delta$  values of (17) and (20).  $\Delta = 400\text{MHz}$  and  $|\Omega_1| = 40\text{MHz}$  are fixed and the different curves are for three different values of the ratio  $|\Omega_0/\Omega_1|$ .

which is solved by

$$\delta \simeq \frac{2\Delta(|\Omega_1|^2 - |\Omega_0|^2)}{8\Delta^2 + |\Omega_0|^2 + |\Omega_1|^2} + \dots, \quad (20)$$

where the ellipsis stands for terms of relative size  $|\Omega/\Delta|^2$  or smaller. The difference between the  $\delta$  values obtained from (17) and (20) can be of the order of a percent ( $\sim (|\Omega_0|^2 + |\Omega_1|^2)/(64\Delta^2)$ ). But the approximate solutions provided by the adiabatic-elimination method do not depend much on this small fractional difference in  $\delta$ . Figure 2 shows the fidelity between the states at later times using the two different values of  $\delta$  when the initial state is  $|0\rangle$ .

The effect of using these two different  $\delta$  values is small when the difference between  $|\Omega_0|$  and  $|\Omega_1|$  is not too large. For the cases shown in Fig. 2, the error from using (17) is a small fraction of a percent. This explains why (17) can serve as a good guidance for experiments, although (20) is more accurate.

### 3.3. Problems with adiabatic elimination

In physics, one speaks of an “adiabatic process” if a relevant property evolves quite slowly, whereas other processes are fast — a clear separation of time scales is a defining element. In the context of adiabatic elimination, one invokes such a separation in the evolution of the components of  $\Psi_I(t)$ , for which we have the Schrödinger equation in (7). One standard argument observes that, as a consequence of  $|\Delta| \gg |\Omega_0|, |\Omega_1|$ , the amplitude  $c_e(t)$  will undergo many oscillations during a period in which  $c_0(t)$  and  $c_1(t)$  do not change substantially. Then, if our interest is not in the short-time changes that would reveal the rapid oscillations of  $c_e(t)$  but predominantly in the longer-time changes of  $c_0(t)$  and  $c_1(t)$ , the average change of  $c_e(t)$  over these longer periods is expected to be quite small. In the spirit of this reasoning, we should then read (9) as a statement about coarse-grained values of the probability amplitudes.

This is hardly a rigorous argument, and whether one regards it as convincing or not is largely a matter of taste. Clearly, though, a more solid argument would be welcome, and one has been provided in (7). Indeed, the reasoning in (7) uses coarse graining in conjunction with a Markov approximation.

There are other problems that one needs to keep in mind when employing adiabatic elimination. We present them as four questions.

- (i) Which is the correct interaction picture to use? The theory argues that the change of the

(coarse-grained) population in the excited state is approximately zero and we arrived at (9) by using the Schrödinger's equation of motion with the time-independent Hamiltonian  $H_I$  in (6). However, the choice of interaction picture is not unique and why do we apply the adiabatic elimination in this particular interaction picture instead of another? For example, by adding a constant term, the operator  $H_I + E$  describes the system equally well. But if we use an interaction picture with  $E \neq 0$ , the resultant two-level effective Hamilton operator also changes as  $\Delta$  gets replaced by  $\Delta + E/\hbar$  in (10) with consequential changes in the evolution of  $\psi(t)$ .

This ambiguity in the choice of interaction picture was studied by Brion, Pedersen, and Mølmer with a Green's function formalism (6). It would be premature, however, to claim that the case is closed. Further studies of the choice of interaction picture and a systematic way of performing the adiabatic elimination are presented in a companion paper (7).

- (ii) Is it possible to estimate the population in the eliminated state? This does not have a simple answer because there are problems with the normalization of the wave function. Originally, we have  $\Psi_I(t)^\dagger \Psi_I(t) = 1$ . Then, since  $H_{\text{eff}}$  is hermitian, we also have  $\psi(t)^\dagger \psi(t) = 1$ . Combined with the initial condition  $(c_0, c_1, c_e) = (1, 0, 0)$  this implies  $c_e(t) = 0$  for all  $t$ , which contradicts the basic approximation in (9).
- (iii) Is it possible to regard the adiabatic-elimination approximation as the first in a hierarchy of approximations? This is possible, indeed, as discussed in (7). It turns out that the next approximation in the hierarchy gives a substantial improvement and better quantitative estimates. In addition, it answers the previous question inasmuch as the next approximation provides an estimate for the population in the auxiliary state.
- (iv) Is it possible to avoid the adiabatic elimination without increasing the complexity much beyond the convenient two-level description of (10)? Yes, this is possible, as we demonstrate in Section 4.

#### 4. Without adiabatic elimination

Alternative methods other than adiabatic elimination are also used to solve Raman-transition problems. The most direct way is, of course, to diagonalize the interaction-picture Hamiltonian of (6), and this can be done by hand since the dimensionality of the system is small. But the expressions for the eigenvalues and eigencolumns of  $H_I$  are quite involved and not transparent. An exception is the two-photon transition with vanishing overall detuning,  $\delta = 0$ , when one can identify a dark state and use it to reduce the three-level system to an effective two-level system, which can then be solved exactly rather simply. The dark states are particularly useful in the context of adiabatic population transfer and electromagnetically induced transparency. When the overall detuning is nonzero, however, there is no dark state. Methods of perturbation theory can then be used to find corrections for a small detuning  $\delta$ , but the complexity grows quickly when high accuracy is required.

In this section, we provide a new way of solving the Raman-transition problem. Just like the dark-state method, it gives a compact exact solution for  $\delta = 0$ , and it can solve the  $\delta \neq 0$  case with very high precision and rather little extra effort.

##### 4.1. General methodology

It will be expedient to use a different interaction picture as the one of (5) and (6) that we used for the adiabatic elimination in Section 3.1. Instead, we choose

$$H_0 = \frac{\hbar}{2} \begin{pmatrix} \Delta + \delta & 0 & 0 \\ 0 & 2\omega_1 + \Delta - \delta & 0 \\ 0 & 0 & 2\omega_e - \Delta \end{pmatrix}, \quad (21)$$

and the Hamiltonian in this interaction picture is

$$H_I = \frac{\hbar}{2} \begin{pmatrix} -\Delta - \delta & 0 & \Omega_0 \\ 0 & -\Delta + \delta & \Omega_1 \\ \Omega_0^* & \Omega_1^* & \Delta \end{pmatrix} = \frac{\hbar}{2} \begin{pmatrix} -(\Delta + \delta\sigma_3) & \Omega \\ \Omega^\dagger & \Delta \end{pmatrix}, \quad (22)$$

where the latter way of writing emphasizes the  $3 = 2 + 1$  split into two relevant states and one auxiliary state;  $\sigma_3$  is the standard third Pauli  $2 \times 2$  matrix, and  $\Omega$  and  $\Omega^\dagger$  are the two-component column of Rabi frequencies,

$$\Omega = \begin{pmatrix} \Omega_0 \\ \Omega_1 \end{pmatrix}, \quad (23)$$

and its adjoint row. This change of interaction picture is equivalent to shifting the energy levels of the interaction-picture Hamiltonian in (6) by  $-\hbar\Delta/2$ , an example of the freedom of choice discussed in question (i) in Section 3.3.

We note that the square of  $H_I$ ,

$$H_I^2 = (\hbar M)^2 = \hbar^2(M_0^2 + \epsilon), \quad (24)$$

is the sum of a “big” block-diagonal part,

$$M_0^2 \equiv \frac{1}{4} \begin{pmatrix} (\Delta + \delta\sigma_3)^2 + \Omega\Omega^\dagger & 0 \\ 0 & \Delta^2 + \Omega^\dagger\Omega \end{pmatrix}, \quad (25)$$

and a “small” off-diagonal part

$$\epsilon \equiv -\frac{\delta}{2} \begin{pmatrix} 0 & \sigma_3\Omega \\ \Omega^\dagger\sigma_3 & 0 \end{pmatrix}. \quad (26)$$

Matrix  $M$  denotes a square root of the matrix  $(H_I/\hbar)^2$  and, since for each eigenvalue we have a choice of sign, there are many  $M$ s that are equally good. Any one can be used as a replacement of  $H_I/\hbar$  in even functions of  $H_I$ ; for example, we could choose  $M > 0$  by convention. In particular, then, the unitary evolution matrix in this interaction picture can be written as

$$U(t) = e^{-iH_I t/\hbar} = \cos(Mt) - \frac{i}{\hbar} \frac{\sin(Mt)}{M} H_I. \quad (27)$$

Except for the common physical approximations that enter the modeling of the atom-laser system by a driven three-level system described by the Hamiltonian of (1)–(3), this is an exact  $3 \times 3$  matrix representing the evolution operator.

Instead of diagonalizing the interaction-picture Hamiltonian (22), we can determine the eigenvalues and eigencolumns of  $M^2$ , whose “big plus small” structure, together with the block-diagonal form of  $M_0^2$ , facilitates approximations. We will see the advantage thereof shortly. Let us note that we can position the factor  $H_I$  in the second term of the right-hand-side of (27) equally well to the left of  $\sin(Mt)/M$ , or break up  $\sin(Mt)/M$  and sandwich  $H_I$  between even powers of  $M$ . Since  $[H_I, M^2] = 0$ , such a change in the order of the matrices makes no difference in (27), but slightly different expressions are obtained when approximations are introduced for the trigonometric functions of  $M$ .



#### 4.2. Vanishing overall detuning ( $\delta = 0$ ) — exact solution

When  $\delta = 0$ , we have  $\epsilon = 0$  and

$$M = M_0 = \frac{1}{2} \begin{pmatrix} -\sqrt{\Delta^2 + \Omega\Omega^\dagger} & 0 \\ 0 & \sqrt{\Delta^2 + \Omega^\dagger\Omega} \end{pmatrix}, \quad (28)$$

where the signs are chosen such that  $M \rightarrow H_I/\hbar$  in the  $\Omega \rightarrow 0$  limit. The resulting evolution operator (27) reads

$$U(t) = \cos(M_0 t) - \frac{i}{\hbar} \frac{\sin(M_0 t)}{M_0} H_I. \quad (29)$$

Owing to the block-diagonal structure of  $M_0$ , the original  $3 \times 3$  problem has been converted into an equivalent  $2 \times 2$  problem without introducing any approximation. Clearly, the technical difficulty has been significantly reduced!

The column  $\Omega$  is an eigencolumn of  $\Delta^2 + \Omega\Omega^\dagger$  with eigenvalue  $\Delta^2 + \Omega^\dagger\Omega$ , so that

$$M_0^2 = \frac{1}{4}(\Delta^2 + \Omega^\dagger\Omega) \begin{pmatrix} \frac{\Omega\Omega^\dagger}{\Omega^\dagger\Omega} & 0 \\ 0 & 1 \end{pmatrix} + \frac{1}{4}\Delta^2 \begin{pmatrix} 1 - \frac{\Omega\Omega^\dagger}{\Omega^\dagger\Omega} & 0 \\ 0 & 0 \end{pmatrix} \quad (30)$$

is the spectral decomposition of  $M_0^2$ . This gives

$$\cos(M_0 t) = \cos\left(\sqrt{\Delta^2 + \Omega^\dagger\Omega} t/2\right) \begin{pmatrix} \frac{\Omega\Omega^\dagger}{\Omega^\dagger\Omega} & 0 \\ 0 & 1 \end{pmatrix} + \cos(\Delta t/2) \begin{pmatrix} 1 - \frac{\Omega\Omega^\dagger}{\Omega^\dagger\Omega} & 0 \\ 0 & 0 \end{pmatrix} \quad (31)$$

and likewise for  $\sin(M_0 t)$  in (29). Hence, the exact evolution of the system can be written out analytically. In particular, the population in the excited state  $|e\rangle$  is non-zero. With the atom initially in the ground state  $|0\rangle$ , it is

$$|c_e(t)|^2 = \left| (0 \ 0 \ 1) U(t) \begin{pmatrix} 1 \\ 0 \\ 0 \end{pmatrix} \right|^2 = \frac{|\Omega_0|^2}{\Delta^2 + \Omega^\dagger\Omega} \sin\left(\sqrt{\Delta^2 + \Omega^\dagger\Omega} t/2\right)^2. \quad (32)$$

This exact expression shows that the population in the excited state oscillates with (angular) frequency  $\frac{1}{2}(\Delta^2 + \Omega^\dagger\Omega)^{1/2}$  and the oscillation amplitude can be non-negligible if  $|\Omega_0|^2$  is a sizeable fraction of  $\Delta^2 + \Omega^\dagger\Omega = \Delta^2 + |\Omega_0|^2 + |\Omega_1|^2$ .

We note that the second projection matrix in (30) and (31) projects on the dark state, whose bra has the row  $(-\Omega_1 \ \Omega_0 \ 0)$  (8). An atom prepared in this dark state stays in it, and there is no probability of finding the atom in the excited state at any time. The atom is essentially decoupled from the driving lasers under these circumstances. In this sense, one could regard (29) with (30) as the evolution matrix in the dark-state formalism but this is, in fact, not the case. In the dark-state approach, one diagonalizes  $H_I$ , reduced to a two-dimensional problem after putting the dark state aside, which amounts to choosing one particular square root of  $M_0^2$  from the continuous family of square roots that the degenerate eigenvalue makes available, namely the square root whose eigenvalues and eigencolumns are those of  $H_I/\hbar$ . No such unique  $M_0$  is needed in (29), nor is there any benefit from enforcing a unique square root of  $M_0^2$  by imposing additional criteria. Although in the  $\delta = 0$  case, this equivalence can be established between the new approach and the dark-state approach, the new approach offers more flexibility and it also has a clear advantage when dealing with the  $\delta \neq 0$  case, as we shall see in Section 4.3.

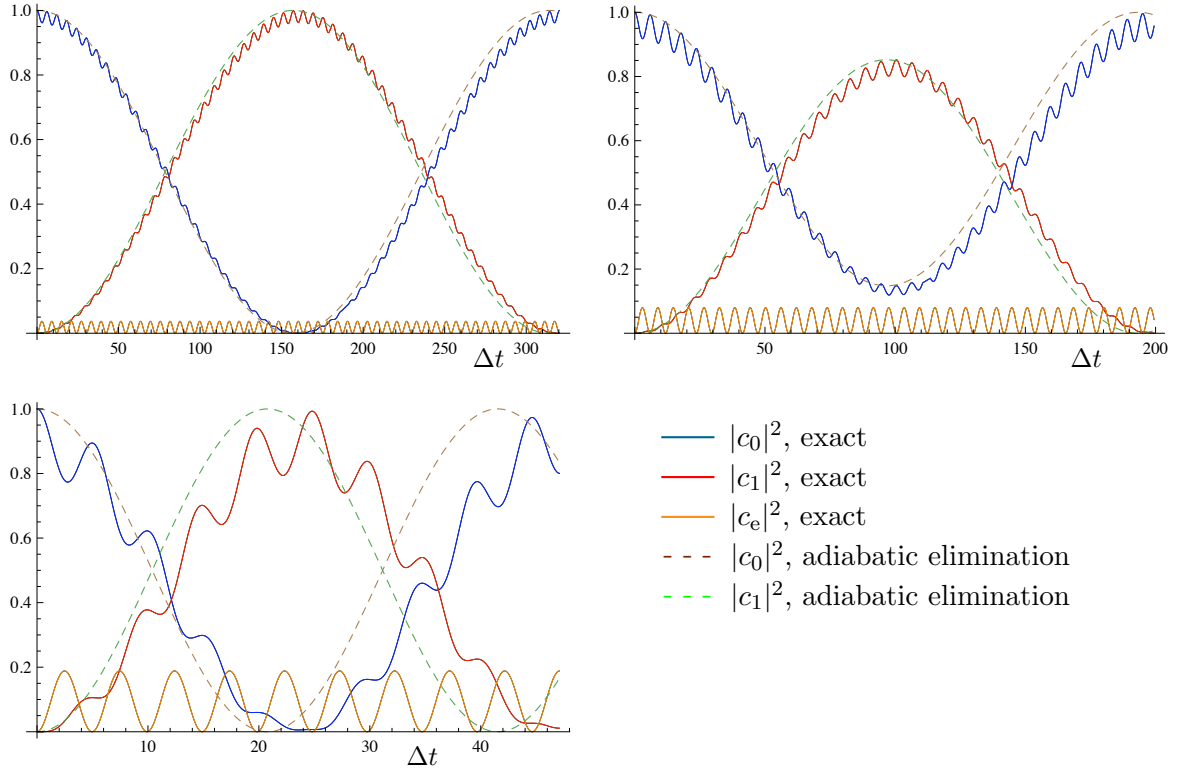


Figure 3. Population distribution for a single-atom Raman transition in time when  $\delta = 0$ . The solid curves show the exact solution, and the dashed curves the adiabatic-elimination approximation. The initial state is  $|0\rangle$ . The red curves are for the ground-state population  $|c_0(t)|^2$ , the blue curves for  $|c_1(t)|^2$ , and the orange curves report  $|c_e(t)|^2$ , the population in the excited state. The detuning is  $\Delta = 400$  MHz for all plots; the top left plot is for  $|\Omega_0| = |\Omega_1| = \Delta/10 = 40$  MHz; the top right plot is for  $|\Omega_0| = \Delta/10 = 40$  MHz and  $|\Omega_1| = \Delta/16 = 25$  MHz; the bottom plot is for  $|\Omega_0| = |\Omega_1| = \Delta/4 = 100$  MHz.

For three sets of parameter values, Fig. 3 shows the population  $|c_e(t)|^2$  of (32) as well as the populations  $|c_0(t)|^2$  and  $|c_1(t)|^2$  of the relevant states  $|0\rangle$  and  $|1\rangle$ . The populations of  $|0\rangle$  and  $|1\rangle$  are oscillating with a slow frequency that goes with a large amplitude and a fast frequency that goes with a small amplitude. The population transfer is predominantly controlled by the slow frequency which, therefore, is the effective Rabi frequency of the system. Since  $M_0^2$  has only two distinct eigenvalues, half the sum of their square roots gives the fast frequency and the difference gives the slow frequency. Thus, we have

$$\Omega_R = \frac{1}{2} \left( \sqrt{\Delta^2 + \Omega^\dagger \Omega} - |\Delta| \right) = \frac{\Omega^\dagger \Omega}{4|\Delta|} - \frac{(\Omega^\dagger \Omega)^2}{16|\Delta|^3} + \dots \quad (33)$$

for the effective Rabi frequency. The expansion in powers of  $|\Omega/\Delta| \ll 1$  permits a comparison of this exact expression with the approximation obtained by adiabatic elimination, the  $\delta = 0$  version of (12): The adiabatic-elimination approximation gives the leading term, but does not reproduce any of the higher-order terms.

In summary, we find that the solution from the adiabatic elimination is indeed the zeroth-order approximation of the exact result in the expansion of  $\Omega^\dagger \Omega / \Delta^2$ . For example, in the zeroth order of  $\Omega^\dagger \Omega / \Delta^2$ , the excited state population vanishes as the oscillation amplitude is proportional to  $\Omega^\dagger \Omega / \Delta^2 \sim 0$ . We conclude that adiabatic elimination yields a reliable approximation only when  $|\Omega_0|, |\Omega_1| \ll |\Delta|$ . The difference between the solutions obtained by our method and the adiabatic-elimination approximation is demonstrated clearly in Fig. 3.

The top left plot in Fig. 3 shows the populations when  $|\Omega_0| = |\Omega_1| = \Delta/10$  is small; in this parameter regime, we can already see the deviation of the adiabatic elimination from the exact result but the deviation is not significant. In the top-right plot, the population of state  $|1\rangle$  only

reaches a maximum of about 80% as  $|\Omega_0| \neq |\Omega_1| \sim \Delta/10$  introduces an effective detuning for the two-photon transition; the adiabatic elimination gives a good approximation since we are still in the regime of  $|\Omega_0|, |\Omega_1| \ll |\Delta|$ . When the magnitudes of  $|\Omega_0|$  and  $|\Omega_1|$  are not much smaller than  $|\Delta|$ , the population of the excited state is no longer negligible, but the complete population transfer between states  $|0\rangle$  and  $|1\rangle$  is still achievable; see the bottom-left plot in Fig. 3. The adiabatic elimination method fails in this case of stronger coupling between the relevant states  $|0\rangle$ ,  $|1\rangle$  and the excited state  $|e\rangle$ .

#### 4.3. Non-zero overall detuning ( $\delta \neq 0$ )

As discussed in Section 3.3, one needs to adjust the detuning  $\delta$  to compensate for the light shifts and achieve complete population transfer from  $|0\rangle$  to  $|1\rangle$ . Besides this, there can also be other experimental reasons for choosing a particular  $\delta$  value. Thus, the situation of  $\delta \neq 0$  is of practical interest, and so we will regard the overall detuning  $\delta$  as a free parameter that is small compared with the average detuning  $\Delta$ . Typically, the ratios  $\delta/\Delta$  and  $\Omega^\dagger\Omega/\Delta^2$  are of the same small order, a few percent perhaps.

The splitting of  $H_1^2$  in (24)–(26) has the diagonal blocks in  $M_0^2$ , including the  $\delta$ -dependent contributions, whereas  $\epsilon$  contains the off-diagonal parts linear in  $\delta$ . We shall treat  $\epsilon$  as a small quantity, without, however, regarding  $\delta$  as an expansion parameter. Rather, the full  $\delta$ -dependence of  $M_0^2$  is taken into account. Then, the eigenvalues of  $M^2$  agree with the eigenvalues of  $M_0^2$  to first order in the perturbation of  $\epsilon$ , and the leading correction will be of order  $\epsilon^2$ .

The eigenvalues of  $M_0^2$  in the subspace spanned by  $|0\rangle$  and  $|1\rangle$  are

$$\mu_\pm^2 = \frac{1}{4}(\Delta^2 + \delta^2) + \frac{1}{8}\Omega^\dagger\Omega \pm \frac{1}{8}\sqrt{(\Omega^\dagger\Omega)^2 + 8\delta\Delta\Omega^\dagger\sigma_3\Omega + (4\delta\Delta)^2}, \quad (34)$$

which we get from diagonalizing the upper  $2 \times 2$  diagonal block  $(\Delta + \delta\sigma_3)^2 + \Omega\Omega^\dagger$ . The unnormalized eigencolumns are

$$\begin{pmatrix} [4\mu^2 - (\Delta + \delta\sigma_3)^2]\Omega \\ 0 \end{pmatrix} \quad \text{for } \mu^2 = \mu_\pm^2, \quad (35)$$

unless  $\Omega$  is an eigencolumn of  $\sigma_3$ , which is a case of no interest. The eigenvalue  $\frac{1}{4}(\Delta^2 + \Omega^\dagger\Omega)$  in the  $1 \times 1$  block for  $|e\rangle$  does not depend on  $\delta$ . With its eigenvalues and eigencolumns at hand, all functions of  $M_0^2$  are readily evaluated.

In passing, we observe that the difference between  $\mu_+^2$  and  $\mu_-^2$  is smallest, as a function of  $\delta$ , when (17) holds, i.e.,  $4\delta\Delta = -\Omega^\dagger\sigma_3\Omega$ . Then

$$\mu_+^2 - \mu_-^2 = \frac{1}{4}\sqrt{(\Omega^\dagger\Omega)^2 - (\Omega^\dagger\sigma_3\Omega)^2} = \frac{|\Omega_0||\Omega_1|}{2}, \quad (36)$$

which is nonzero in all situations of interest.

For a systematic inclusion of correction of orders  $\epsilon$ ,  $\epsilon^2$ ,  $\epsilon^3$ ,  $\dots$ , we do not use the perturbation theory for an approximation of the eigenvalues and eigencolumns of  $M^2$  for use in (27). Rather, we generate approximations for the evolution matrix  $U(t) = \exp(-iH_I t/\hbar)$  itself with the aid of an equation of Lippmann-Schwinger type,

$$U(t) = U_0^{(R)}(t) - \int_0^t dt' \frac{\sin(M_0(t-t'))}{M_0} \epsilon U(t'), \quad (37)$$

where

$$U_0^{(R)}(t) = \cos(M_0 t) - \frac{i}{\hbar} \frac{\sin(M_0 t)}{M_0} H_1 \quad (38)$$

differs from (29) by the inclusion of the  $\delta$  dependent terms in  $M_0$  and  $H_1$ . One way of verifying that (37) is correct, is by checking that both sides have the same Laplace transform. Indeed, they do:

$$\int_0^\infty dt e^{-st} U(t) = \frac{1}{s + iH_1/\hbar} = \frac{s}{s^2 + M_0^2} - \frac{i}{\hbar} \frac{1}{s^2 + M_0^2} H_1 - \frac{1}{s^2 + M_0^2} \epsilon \frac{1}{s + iH_1/\hbar} \quad (39)$$

is an identity that follows from (24).

As mentioned at the end of Section 4.1, the multiplication order of  $H_1$  and even powers of  $M^2$  is irrelevant in (27) as they commute. In (38), however, the order does matter as  $[H_1, M_0^2] \neq 0$  when  $\delta \neq 0$ . In addition to (37) with (38) where  $H_1$  is on the right, we have, therefore, also an “on the left” version,

$$U(t) = U_0^{(L)}(t) - \int_0^t dt' U(t-t') \epsilon \frac{\sin(M_0 t')}{M_0} \quad (40)$$

with

$$U_0^{(L)}(t) = \cos(M_0 t) - \frac{i}{\hbar} H_1 \frac{\sin(M_0 t)}{M_0}. \quad (41)$$

Half their sum gives a symmetrized version,

$$U(t) = U_0^{(S)}(t) - \frac{1}{2} \int_0^t dt' \frac{\sin(M_0(t-t'))}{M_0} \epsilon U(t') - \frac{1}{2} \int_0^t dt' U(t-t') \epsilon \frac{\sin(M_0 t')}{M_0} \quad (42)$$

with

$$U_0^{(S)}(t) = \cos(M_0 t) - \frac{i}{2\hbar} \frac{\sin(M_0 t)}{M_0} H_1 - \frac{i}{2\hbar} H_1 \frac{\sin(M_0 t)}{M_0}, \quad (43)$$

and there are many more variants that one could explore.

Each of the integral equations (37), (40), and (42) provides a hierarchy of approximations by an iteration that commences with the respective zeroth-order approximation. This is, of course, the procedure by which one generates the Born series from the Lippmann-Schwinger equation. For the “on the right” equation (37), the  $k$ th-order approximation is

$$U_k^{(R)}(t) = U_{k-1}^{(R)}(t) - \int_0^t dt' \frac{\sin(M_0(t-t'))}{M_0} \epsilon U_{k-1}^{(R)}(t'), \quad (44)$$

and analogous expressions apply to the “on the left” version and the symmetrized variant. Note that  $U_k^{(S)}(t)$  is not half the sum of  $U_k^{(R)}(t)$  and  $U_k^{(L)}(t)$  for  $k \neq 0$ ; that arithmetic mean could also be taken as a valid  $k$ th-order approximation. For such a scheme to be useful in practice, the zeroth-order approximation should be quite good to begin with, the first-order approximation should be sufficient for many purposes, and it should not be necessary to go beyond the second order.

The various  $k$ th-order approximations differ from each other, but they are all accurate up to  $k$ th-order in  $|\epsilon/M_0^2| \sim |\delta\Omega|/\Delta^2$ . In the common case where  $|\Omega/\Delta| \sim 10^{-1}$  and  $|\delta/\Delta| \sim 10^{-2}$ , we

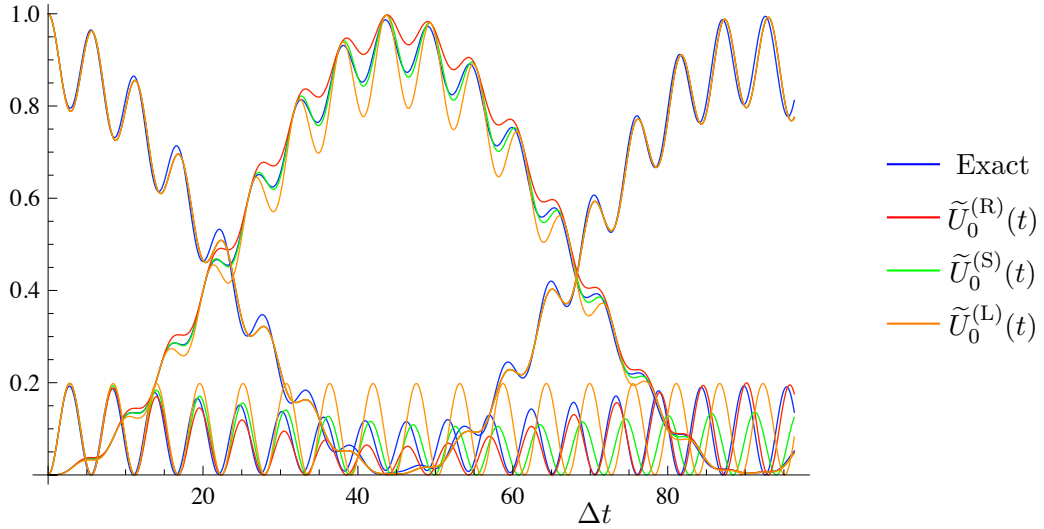


Figure 4. Plots of populations obtained from different zeroth-order solutions of the Lippmann-Schwinger equations. Blue curves give the exact results from numerical simulation using the Hamiltonian  $H_I$ ; green curves show solutions from the symmetric approximation  $\tilde{U}_0^{(S)}(t)$ ; red curves show solutions from  $\tilde{U}_0^{(R)}(t)$ ; and orange curves show solutions from  $\tilde{U}_0^{(L)}(t)$ . The parameters are  $\Delta = 400$  MHz,  $|\Omega_0| = \Delta/2$ ,  $|\Omega_1| = 3\Delta/10$  and  $\delta = -\Omega^\dagger \sigma_3 \Omega / (4\Delta) = (|\Omega_1|^2 - |\Omega_0|^2) / (4\Delta) = -16$  MHz. The effective Rabi frequency is  $\Omega_R = 27.8$  MHz, about 7% of  $\Delta$ . Initially, we have  $c_0(0) = 1$  and  $c_1(0) = c_e(0) = 0$ . The curves starting at 1 show the approximations for  $|c_0(t)|^2$ ; the curves that start at 0 and rise to 1 are for  $|c_1(t)|^2$ ; and the curves that start at 0 and never exceed small values are for  $|c_e(t)|^2$ .

have  $|\epsilon/M_0^2| \sim 10^{-3}$ . Remember that the  $\delta$  dependence in  $H_I$  and the  $\epsilon$  dependence (which also depends on  $\delta$ ) are treated separately. Although  $\epsilon$  goes to zero when  $\delta$  vanishes,  $|\epsilon/M_0^2|$  is one order of magnitude smaller than  $|\delta/\Delta|$ .

A technical point is the following. The approximate evolution matrices  $U_k(t)$  are not unitary, rather  $U_k(t)^\dagger U_k(t)$  deviates from the unit matrix by an amount of order  $\epsilon^{k+1}$ . One can cope with this in various ways (11). Perhaps the simplest is to ensure proper normalization by including a time-dependent factor that depends on the initial set of probability amplitudes, thereby arriving at an effectively unitary matrix  $\tilde{U}_k(t)$  that is suitable for the given initial column  $\Psi_I(0)$ ,

$$\tilde{U}_k(t)\Psi_I(0) = \frac{U_k(t)\Psi_I(0)}{\sqrt{\Psi_I(0)^\dagger U_k(t)^\dagger U_k(t)\Psi_I(0)}}. \quad (45)$$

In other words, we apply  $U_k(t)$  to  $\Psi_I(0)$  and normalize the resulting column to unit length. This procedure worked fine for all examples that we studied.

As remarked above, the  $k$ th-order approximations  $U_k^{(R)}(t)$ ,  $U_k^{(L)}(t)$ , and  $U_k^{(S)}(t)$  differ slightly and might not describe the system equally well. We discuss a few examples of the state populations as functions of time under the different approximations, and analyze their performance. We compare the results to the exact numerical answers. The value  $\Delta = 400$  MHz is taken for the average detuning, as it is of typical order for real experiments, and the values of the Rabi coupling strengths  $\Omega_0$  and  $\Omega_1$  can vary in a range of fractions of  $\Delta$ . The overall detuning  $\delta$  of the two-photon transition can be controlled to within 1 MHz accuracy in laboratory experiments. For the purpose of this analysis, then, we take the liberty of setting  $\delta$  to any value we like.

Figure 4 gives an example that demonstrates the quality of the zeroth-order approximations given by  $\tilde{U}_0^{(R)}(t)$ ,  $\tilde{U}_0^{(L)}(t)$ , and  $\tilde{U}_0^{(S)}(t)$ . Since  $U_0^{(S)}(t)$  is an average of  $U_0^{(R)}(t)$  and  $U_0^{(L)}(t)$ , we expect the population curves for  $\tilde{U}_0^{(S)}(t)$  to lie between the other two curves and this can be seen quite clearly in Fig. 4. Moreover, the solutions of the population in the initial state  $|0\rangle$  do not depend much on which of the three zeroth-order approximations is used, and all of them are very close to the exact numerical solution. In this example, we use  $\delta = (|\Omega_1|^2 - |\Omega_0|^2)/(4\Delta)$ , the value of (17), which gives an effective resonant two-photon transition, and we can see that

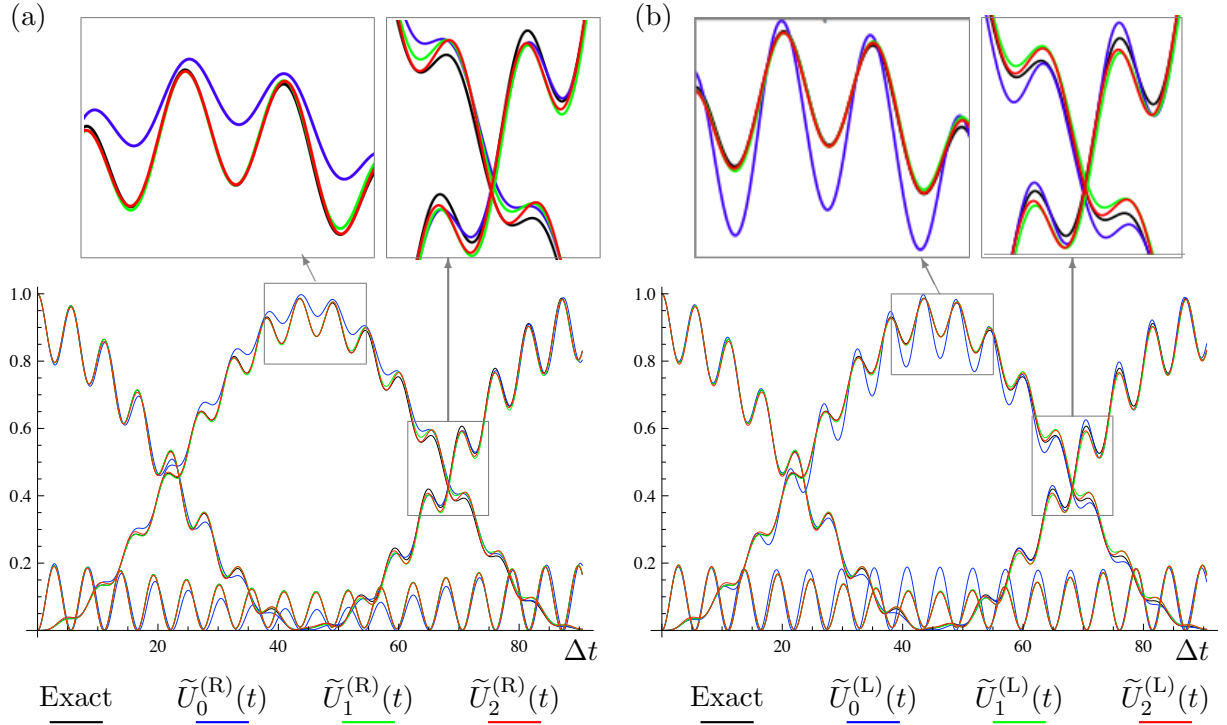


Figure 5. Comparison of the probabilities obtained from the zeroth-, first-, and second-order approximations of the Lippmann-Schwinger equations (37) and (40). In plot (a), the blue, green, and red curves show solutions from  $\tilde{U}_0^{(R)}(t)$ ,  $\tilde{U}_1^{(R)}(t)$ , and  $\tilde{U}_2^{(R)}(t)$ , respectively; and in plot (b), the blue, green, and red curves show solutions from  $\tilde{U}_0^{(L)}(t)$ ,  $\tilde{U}_1^{(L)}(t)$ , and  $\tilde{U}_2^{(L)}(t)$ , respectively. The parameters and the initial state are the same as in Fig. 4.

full population transfer from  $|0\rangle$  to  $|1\rangle$  can be achieved. In comparison, full population transfer cannot be achieved for other values of  $\delta$ .

In Fig. 4, the value of  $|\delta|$  is about a few percent of  $|\Delta|$ . The plot shows that, in this parameter regime,  $\tilde{U}_0^{(S)}(t)$  approximates the evolution of the probabilities for finding  $|0\rangle$  and  $|1\rangle$  quite well, and it certainly works best among the three different zeroth-order approximations shown here. The approximation for the excited state population also works well when  $t$  is short, i.e., during the first few fast oscillation periods, but the deviation grows quickly with time.

The accuracy is better for higher-order approximations. We compare the approximations of zeroth, first, and second order for the three different Lippmann-Schwinger equations in Figs. 5(a), 5(b), and 6. Figure 5(a) shows that the deviation of the zeroth-order approximation  $\tilde{U}_0^{(R)}(t)$  from the exact numerical solution is large when about half of the effective Rabi cycle is completed, i.e., around  $t = \pi/\Omega_R$  or  $\Delta t \simeq 45$ , and the deviation is smaller around a full Rabi cycle. The main deviation is in the size of the small-amplitude oscillations with short period, whereas the Rabi oscillation with longer period is reproduced equally well by  $\tilde{U}_k^{(R)}(t)$  with  $k = 0, 1, 2$ . The first-order approximation corrects part of the error in the zeroth-order approximation, and the second-order approximation improves matters further and gets the probabilities very close to their exact values. The same observations can be made about the corresponding “on the left” approximations in Fig. 5(b). How about the symmetric version  $\tilde{U}_k^{(S)}(t)$  whose zeroth-order approximation already works quite well?

Figure 6 shows that when the two-photon transition is resonant, the difference between  $\tilde{U}_0^{(S)}(t)$ ,  $\tilde{U}_1^{(S)}(t)$ , and  $\tilde{U}_2^{(S)}(t)$  is difficult to detect. All three lowest-order approximations of (42) describe the evolution of the system well during the first Rabi cycle. The zeroth-order approximation works surprisingly well, at times it gives a better result than the higher-order approximations (see the bottom plot of the two blow-ups). The improvement offered by the higher-order approximations can be observed near the middle of the Rabi cycle (see the top plot of the blow-ups),

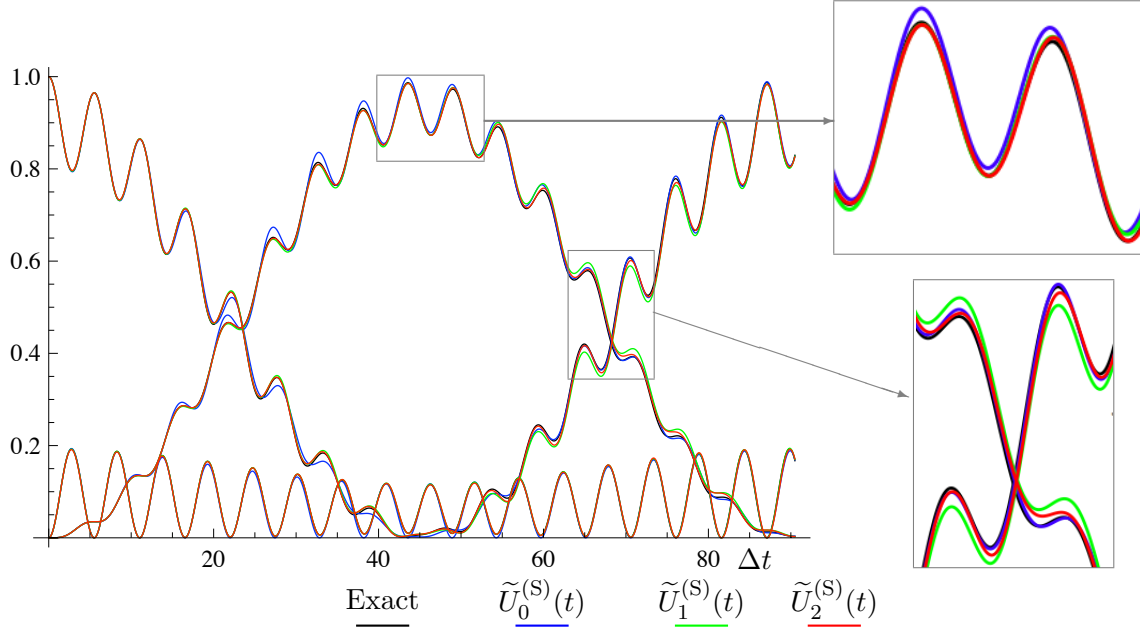


Figure 6. Comparison of the zeroth-, first-, and second-order approximations of the symmetric Lippmann-Schwinger (42). The parameter values, the initial state, and the color coding are the same as in Fig. 5.

and this improvement is more substantial when  $\epsilon$  gets larger. For a practical application to experiments that aim at complete population transfer from  $|0\rangle$  to  $|1\rangle$ , the approximation provided by  $\tilde{U}_0^{(S)}(t)$  is accurate enough to determine the parameter values reliably.

#### 4.4. Discussion

To summarize our approach, we split  $(H_I/\hbar)^2$ , the square of the interaction Hamiltonian, into two parts: the dominant part  $M_0^2$  and a small correction  $\epsilon$ . With this splitting and any one of the Lippmann-Schwinger equations (37), (40), or (42), successive approximations to the unitary evolution matrix  $U(t) = \exp(-iH_I t/\hbar)$  can be obtained iteratively. If we use the approximations given by  $\tilde{U}_k^{(R)}(t)$  and  $\tilde{U}_k^{(L)}(t)$ , we only need to do one iteration and stop at the first-order solution ( $k = 1$ ) for a very good approximation. If we use the symmetric version  $\tilde{U}_k^{(S)}(t)$ , we do not even need to go beyond the zeroth-order approximation since  $\tilde{U}_0^{(S)}(t)$  is already very close to the exact evolution for typical experimental parameters. Thus, we have

$$U(t) \simeq U_0^{(S)}(t) = \cos(M_0 t) - \frac{i}{2\hbar} \frac{\sin(M_0 t)}{M_0} H_I - \frac{i}{2\hbar} H_I \frac{\sin(M_0 t)}{M_0} \rightarrow \tilde{U}_0^{(S)}(t), \quad (46)$$

where  $\tilde{U}_0^{(S)}(t)$  differs from  $U_0^{(S)}(t)$  by the time-dependent factor of (45) that ensures  $\Psi_1(t) = \tilde{U}_0^{(S)}(t)\Psi_1(0)$  is properly normalized for the given initial column of probability amplitudes.

According to (46), the oscillation of the state populations of  $|0\rangle$  and  $|1\rangle$  are governed by the operator  $M_0^2$ . The effective Rabi oscillation frequency, to a very good approximation, only depends on the eigenvalues  $\mu_{\pm}^2$  of the first diagonal block of  $M_0^2$ . Applying the same argument as in Section 4.2 for the case of  $\delta = -\Omega^\dagger \sigma_3 \Omega / 4\Delta$  in (17), the effective Rabi frequency is (we take  $\mu_{\pm} > 0$ )

$$\Omega_R = \mu_+ - \mu_- = \frac{1}{2} \sqrt{(\Delta^2 + \delta^2) + \frac{1}{2}(|\Omega_0| + |\Omega_1|)^2} - \frac{1}{2} \sqrt{(\Delta^2 + \delta^2) + \frac{1}{2}(|\Omega_0| - |\Omega_1|)^2}. \quad (47)$$

With this particular choice of  $\delta$ , the Rabi oscillation amplitude could reach unity; however, this

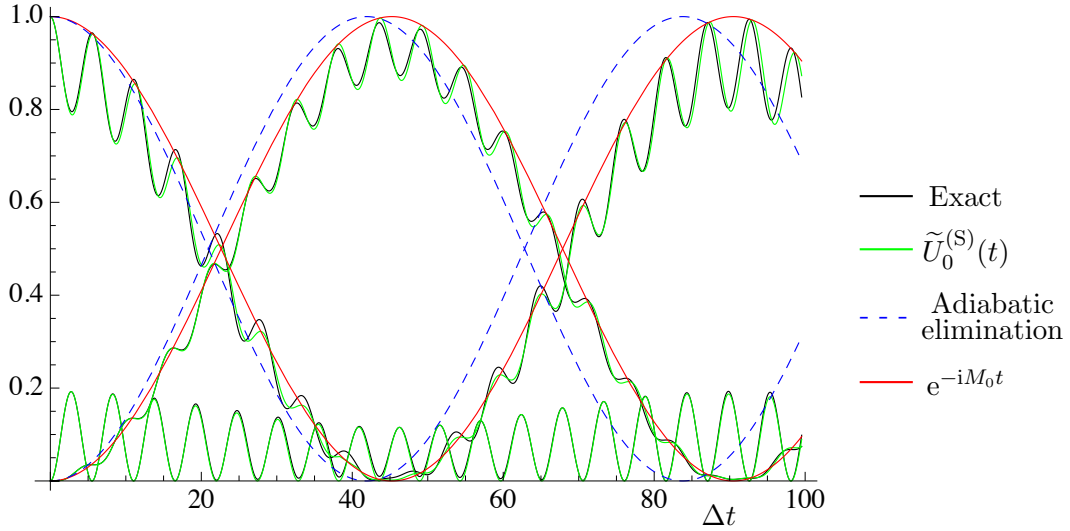


Figure 7. Improvement on the effective two-level Hamiltonian compared with adiabatic elimination. The black curves give the exact numerical solution; the green curves are for the symmetric zeroth-order approximation of  $U(t)$ ; the blue dashed curves are for the adiabatic-elimination approximation; and the red curves result from taking  $M_0$  as the effective Hamiltonian. The parameters are the same as in Fig. 4.

might not be the real maximum that the population in state  $|1\rangle$  can reach, because on top of this slow effective Rabi oscillation, the population also oscillates with a fast frequency. This fast oscillation goes roughly with the frequency  $\mu_+ + \mu_- \simeq |\Delta|$ . Nevertheless, up to linear order in  $\delta/\Delta$ , we find that the oscillation amplitude goes to unity, regardless whether we choose  $\delta$  in accordance with (17) or with (20). This shows why the evolution of the system is essentially the same for both  $\delta$  values.

Moreover, since the effective Rabi oscillation of the two relevant states depends on the eigen-system of  $M_0^2$  only, the effective Hamiltonian between states  $|0\rangle$  and  $|1\rangle$  is approximately given by the  $2 \times 2$  upper diagonal block of  $\hbar M_0$ , if we exclude the excited state  $|e\rangle$  from the evolution directly. That is

$$H_{\text{eff}} = -\frac{\hbar}{2} \sqrt{(\Delta + \delta\sigma_3)^2 + \Omega\Omega^\dagger}. \quad (48)$$

The minus sign is chosen with the same reasoning as in (28). From this effective Hamiltonian, we can find the Rabi frequency directly and one of the special cases was already given in (47); the oscillation amplitude for an arbitrary  $\delta$  is

$$P = 1 - \frac{(\Omega^\dagger\sigma_3\Omega + 4\delta\Delta)^2}{(\Omega^\dagger\Omega)^2 + 8\delta\Delta\Omega^\dagger\sigma_3\Omega + (4\delta\Delta)^2}, \quad (49)$$

and again we have  $P = 1$  when  $\delta = -\Omega^\dagger\sigma_3\Omega/4\Delta$ . Figure 7 shows that this effective Hamiltonian is much more accurate than that of the adiabatic-elimination approximation, inasmuch as the evolution by  $e^{-iM_0t}$  gives a very close envelope of the population oscillation.

## 5. Summary and Outlook

After reviewing the standard adiabatic-elimination approximation, which reduces the theoretical description of a three-level Raman transition to an effective two-level problem, and identifying some of the shortcomings of this approach, we introduced an alternative approximation method. Similarly to adiabatic elimination, there is an essential two-level component in the new method without, however, eliminating the third auxiliary level. This makes the new method



easy to use, inasmuch as one only needs to diagonalize a  $2 \times 2$  matrix. Integro-differential equations of Lippmann-Schwinger type are the powerful tools that enable us to generate successive approximations. A particular one with high symmetry performs so well that the lowest-order approximation is all one needs for a highly reliable determination of experimental parameters.

For the sake of simplicity in presentation, the discussion was here limited to two-photon transitions. The method can also be applied to more complicated situations (11), about which we will report on another occasion.

## Acknowledgments

This work is supported by the National Research Foundation and the Ministry of Education, Singapore. We are grateful for insightful discussions with Vanessa Paulisch, Antoine Browaeys, János Bergou, Gerd Leuchs and Björn Hessmo.

## References

- (1) Scully, M. O.; Zubairy M. S. “Quantum Optics” **1997**, *Cambridge University Press*.
- (2) Kyrölä, E.; Lindberg, M. *Phys. Rev. A* **1987**, *35*, 4207–4225.
- (3) Kyrölä, E.; Lindberg, M. *Opt. Commun.* **1983**, *48*, 284–286.
- (4) Oreg, J.; Hioe, F. T.; Eberly, J. H. *Phys. Rev. A* **1984**, *29*, 690–697.
- (5) Kuklinski, J. R.; Gaubatz, U.; Hioe, F. T.; Bergmann, K. *Phys. Rev. A* **1989**, *40*, 6741–6744.
- (6) Brion, E.; Pedersen, L. H.; Mølmer, K. *J. Phys. A: Math. Theo.* **2007**, *40*, 1033–1043.
- (7) Paulisch, V.; Han, R.; Ng, H. K.; Englert, B.-G. **2012** (Posted simultaneously on the arXiv).
- (8) Fleischhauer, M.; Manka, A. S. *Phys. Rev. A* **1996**, *54*, 794–803.
- (9) Miroshnychenko, Y.; Gaëtan, A.; Evellin, C.; Grangier, P.; Comparat, D.; Pillet, P.; Wilk, T.; Browaeys, A. *Phys. Rev. A* **2010**, *82*, 013405.
- (10) Barratt, J. P.; Cohen-Tannoudji, C. *J. Phys. Radium* **1961**, *22*, 329 and 443.
- (11) Han, R. *Ph.D. Thesis* “Robust Quantum Storage With Three Atoms” **2012**, National University of Singapore.